METHOD DEVELOPMENT AND PERFORMANCE STUDY OF GEANT4 AND GOLD'S ALGORITHM FOR GAMMA SPECTRAL UNFOLDING

A Thesis
Presented to
The Academic Faculty

by

Wesley C. Gillis

In Partial Fulfillment
of the Requirements for the Degree
Master's of Science in the
School of Mechanical Engineering

Georgia Institute of Technology
May 2018

METHOD DEVELOPMENT AND PERFORMANCE STUDY OF GEANT4 AND GOLD'S ALGORITHM FOR GAMMA SPECTRAL UNFOLDING

Approved by:

Dr. Anna Erickson, Advisor
Committee Chair
Georgia Institute of Technology

Dr. Nolan Hertel
School of Mechanical Engineering
Georgia Institute of Technology

Dr. Steven Biegalski
School of Mechanical Engineering
Georgia Institute of Technology

Date Approved: 23 January 2018

ACKNOWLEDGEMENTS

I want to thank my advisor, Dr. Erickson, for her continuous support. I'd also like to thank my colleagues John, Andrew, Joe, Colin, Jake, Luke, Greg, and Paul for their invaluable discussions and help.

I'd like to also thank Jin, my mom, my dad, my aunt, my brother, my cousin, and grandparents for all their love and support.

This research was performed under appointment to the Nuclear Nonproliferation International Safeguards Fellowship Program sponsored by the National Nuclear Security Administration's Office of International Nuclear Safeguards (NA-241).

TABLE OF CONTENTS

LIST OF TABLES

LIST OF FIGURES

SUMMARY

This thesis focuses on the development and implementation of a method to unfold the gamma energy distribution incident on a detector from that detector's inherent response. A common assumption is made to tackle this problem: the response of the detector is a linear transformation of the incident gamma distribution that maps to the actual measurement. This problem is simplified into an inverse matrix problem, where Gold's iterative matrix-unfolding algorithm is used for this deconvolution. The response function matrix is created using a semi-empirical technique where Monte Carlo simulations are coupled with information extracted from experimental data. To determine the capabilities of this approach, the model used to generate the matrix is verified against experiment. Once ready for unfolding, both a performance metric of the algorithm and a selection method for the algorithm's parameters are designed with consideration to their physical implications. Finally, these various methods are applied to five spectra: ^{137}Cs, ^{60}Co, ^{22}Na, PuBe, and the resulting gamma spectrum from a cyclotron-induced reaction.

CHAPTER I

INTRODUCTION

Knowing the gamma energy distribution of some radiation field in great detail has a vast number of applications. Such instances include characterizing an unknown source, identifying an isotope with unique gamma signatures, or determining how a gamma energy distribution changes when passing through some material. Applications for gamma spectroscopy are seemingly endless, including medical imaging, nonproliferation, radiation protection, dosimetry, and safeguards, to name a few.

In particular, the application of gamma spectroscopy to nonproliferation is of high interest in today's research landscape. In the active interrogation of cargo scanning, previous approaches use bremsstrahlung-based sources for imaging. However, new methods propose to replace these sources with a low-energy nuclear reaction (LENR) source for various reasons. First, these proposed sources have higher mean energies than typical bremsstrahlung beams, making them more highly penetrating. Additionally, the reduction in low energy photons that are normally absorbed by the cargo reduces the absorbed dose to the cargo. Some of these reactions also produce neutrons, which can be useful if probing for special nuclear material. The discrete nature of the gamma ray energies, as opposed to a continuous bremsstrahlung spectrum, can also be exploited for higher information gain.

One LENR of interest is $^{11}B(d,\gamma n)^{12}C$, where deuterons around 3 MeV are accelerated onto a ^{11}B target. The measured gamma spectrum from such an accelerator at MIT is shown in Figure 1. Several of the gamma lines are expected from ^{12}C nuclear transitions, particularly 4.438 MeV and 15.1 MeV. These gammas are particularly useful for cargo scanning purposes because the relative transmission of these gammas

through a material will allow not only the determination of material density, but also effective atomic number [17]. Thus, knowing the expected emission probabilities of these gamma lines is important for the design and optimization of a cargo scanning system using this beam.

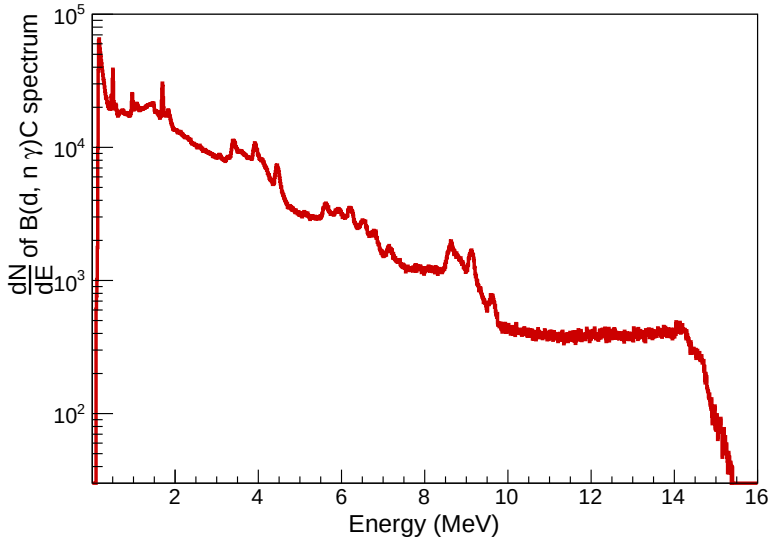

Figure 1: $LaBr_3(Ce)$ measurement of the gamma spectrum from $^{11}B(d,\gamma n)^{12}C$ [18].

The expected population of ^{12}C states and the subsequent transition probabilities, however, are not well known. Analyzing a measured gamma spectrum like the one in Figure 1 can give insight into the relative state populations, but not without some level of post-processing. The true energy distribution of the gammas is not shown, but a convoluted spectrum due to the detection mechanisms used to measure it. Determining the incident distribution is the motivation behind this thesis, where the approach is gamma spectral unfolding. This common method estimates the detector's response to a range of gamma energies, then attempts to mathematically separate the response from the incident distribution.

Gamma unfolding has been in the literature for many decades, though the computational power available today has only recently become available. Simulating a response function with gammas up to 16 MeV allows the extension of these age-old

techniques to newer problems such as the LENR in Figure 1. Using the guidance of a combination of these previous approaches, a methodology is developed for the response function creation for both 5 MeV and 16 MeV max-energy applications. Subsquently, an particular algorithm for unfolding is needed, along with an evaluation of the response function model and the unfolded spectra.

1.1 Objective

The overall goal of this work is to unfold gamma spectra with energies below 5 MeV and the LENR spectrum in Figure 1. Several objectives are necessary to achieve meaningful results.

1. Design, implement, and test an approach to create a response function matrix that sufficiently represents the response of $LaBr_3(Ce)$ to a wide range of incident gamma energies.

2. Select and apply an algorithm that is capable of deconvolving the response function from measurements without oscillating.

3. Develop a performance metric to determine the quality of the unfolded spectrum.

4. Develop a strategy for the selection of algorithm performance parameters using the performance metric.

5. Apply these methods to the spectra of interest, using the results as a final evaluation of the overall approach.

CHAPTER II

TECHNICAL BACKGROUND

2.1 Gamma Spectrum Unfolding

Energy spectrum unfolding is the mathematical attempt to separate a radiation detector's characteristic response from the energy distribution that was incident upon it. When a detector measures gamma rays of a certain energy, E, the response of the detector is not an impulse at E. Rather, it is a function of the various gamma interactions that produce energetic electrons in the material. Beyond this variation in electron energy, the number of informations carriers that are created, the collection efficiency of these information carriers, and the subsequent electronics play a significant role in the response of an individual system. If the incident energy distribution is not monoenergetic, but rather a distribution, determining this distribution is an ill-conditioned inverse problem [13].

There have been several approaches to gamma spectrum unfolding, most of which rely on the predictable features of gamma spectra to facilitate the unfolding process. Two semi-analytical methods include the folding iteration method and the stripping method. Both attempt to remove the Compton scattering contribution by iterating through the spectrum multiple times [8] [19]. This approach is effective for detectors with good energy resolution and a well-defined full-energy-peak. In these cases, the spectrum after processing is just the full-energy deposition peaks, but they do not account for single and double escape peaks in higher energy spectra. Another more recent approach is unfolding using artificial neural networks, which is trained experimental data to recognize patterns in the spectra in attempt to either identify isotopes or to output the incident photon spectrum [1]. Using this machine learning approach

requires a large dataset to train the network that properly represent the energy-space of interest [12].

The iterative matrix-unfolding method is a common unfolding approach that uses a response function matrix to extract the unfolded spectrum. The matrix represents how a particular detector would respond to different incident photon energies. A challenge of this method is in generating the response matrix. One study uses several monoenergetic gamma sources to generate a small subset of the response matrix, then interpolates spectra in between the experimental matrix to fill out the matrix [8]. When using experimental data as the foundation for the matrix construction, interpolation is an integral step to ensuring that the matrix spans the energy-space. Another approach to complete a full matrix is through simulation. This is either done by finely sampling the energy-space [16] or sampling a smaller subset of energies coupled with interpolation [10]. Simulation of detector response can also have a variety of levels of complexity, e.g. simulating the scintillation yields or electron-hole pair transport or simply energy deposition in the detector. For each, empirical data is necessary to supplement the simulations. This is in the form of either information carrier production and propagation or the macroscopic characterization of energy resolution.

2.1.1 Iterative Matrix-Unfolding Method

A measured detector response $y(E)$ is formulated as

$$y(E) = \int_0^\infty R(E')x(E')dE' \tag{1}$$

This continuous representation is often simplified to a linear system for a variety of solution methods. To do this, the iterative matrix-unfolding method assumes that the total response of a detector is a linear combination of the responses to all the photon energies incident on the detector volume. In other words, an experimental spectrum

(y) results from taking the incident energy spectrum (x) and linearly transforming it via the response function $(\mathbf{R})$, or $\mathbf{R} : x \rightarrow y$. The general equation for this method is shown in Eq. 2. The goal here is to determine the unfolded spectrum, which is x.

$$y = \mathbf{R} \cdot x \tag{2}$$

This equation can be written in a more explicit form as in Eq. 3. This describes a matrix where the unfolded spectrum x has M elements, and the measured experimental spectrum has N elements.

$$y(E_i) = \sum_{k=0}^{M-1} \mathbf{R}(E_i, E_k) x(E_k), i = 0, 1, 2, ..., N-1 \tag{3}$$

Solving for x, however, requires a matrix-unfolding method. To do this, an implementation of the Gold Decomposition Algorithm from ROOT is used.

2.1.2 Gold Decomposition Algorithm

The algorithm used for the decomposition is part of the ROOT code package. ROOT is an open-source package developed originally for high energy physics analysis [4]. The specific details of this implementation are referenced from [10], and the algorithm details are discussed in the original paper by Gold [7]. Its primary merit is that it guarantees a non-oscillating solution. The first step in solving Eq. 2 is to find the vector z by

$$z = \mathbf{A} \cdot x \tag{4}$$

where $\mathbf{A} = \mathbf{R}^T \mathbf{R}$ and $z = \mathbf{R}^T \cdot y$. The method iteratively solves for x using Eq. 5.

$$x_i^{(k+1)} = x_i^{(k)} + \frac{x_i^{(k)}}{\sum_{m=0}^{N-1} \mathbf{A}_{im} x_m^{(k)}} \left[z_i - \sum_{m=0}^{N-1} \mathbf{A}_{im} x_m^{(k)} \right] \tag{5}$$

This is performed for some number of iterations $k = 0, 1, ..., L$. The algorithm starts with initial solution

$$x^{(0)} = [1, 1, ..., 1]^T. \tag{6}$$

This method is positive definite and converges to some stable state. Additional iterations past convergence do not provide further results. ROOT's implementation, however, provides a boosting option for the algorithm to continue to decrease the deconvolved peak widths. The description of this process is again referenced from [10]:

1. Set the initial solution $x^{(0)}$ according to Eq. 6.
2. Set the required number of repetitions R and iterations L.
3. Let number of repetitions r = 1.
4. According to Eq. 5 for $k = 0, 1, ..., L-1$ find solution $x^{(L)}$.
5. If $r = R$ finish the calculation, else
   (a) apply boosting operation, i.e. set $x_i^{(0)} = \left|x_i^{(L)}\right|^p$ $i = 0, 1, ..., N-1$ and p is boosting exponent;
   (b) set $r = r + 1$;
   (c) continue in 5.

2.2 Energy Calibration and Resolution in $LaBr_3(Ce)$

An understanding of the behavior of inorganic scintillators is necessary for the semi-empirical approach used for spectral unfolding for two reasons. First, the experimental spectrum must be calibrated to energy because the simulation outputs in energy units, and second, the energy resolution information is used in the creation of the response function.

The calibration technique maps channel number to energy using known gamma spectra. Fitting the calibrations with some function, as in Figure 2, allows the experimental spectrum to be transformed into energy-space. The calibration is not, however, linear in energy. This can occur from saturation in the PMT [15] and from the increase in ionization density in the electron track with decreasing electron energy causing non-proportionality [5].

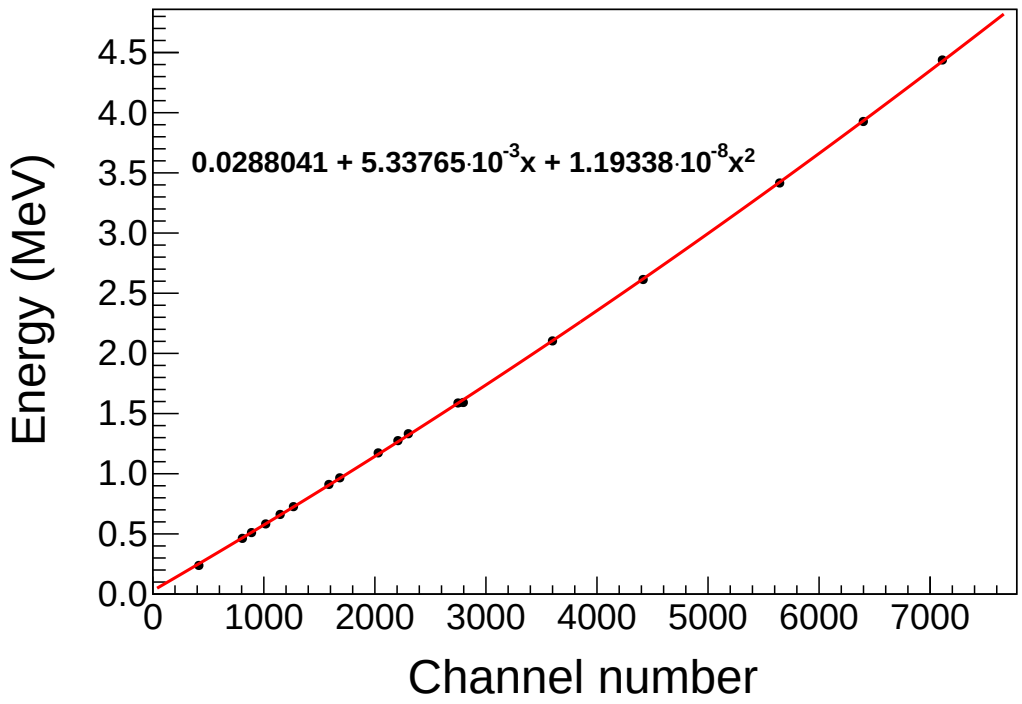

Figure 2: The energy calibration curve relates the voltage channels from the multichannel analyzer to the corresponding electron energy. The voltage pulse created in a scintillator is assumed represent the energy deposited in the detector by the charged particle that induced the signal. This relationship is sometimes nonlinear due to PMT saturation [15] and non-proportionalities in ionization densities [5].

After the calibration, the energy resolution information needed for the response function matrix can be extracted, explained in detail in Section 3.1. To do this, it is assumed that the full-energy deposition peaks are Gaussian. Using the standard deviation from Gaussian functions fit to the data works for most gamma sources,

but there is an issue when applied to reaction-based sources. When a nuclear reaction produces gammas, they are broadened in energy due to the kinematics of the reaction [14]. The width of the experimental peak from a broadened gamma is not representative of the intrinsic energy resolution of the detector at that energy.

2.2.1 Energy Broadening from Reaction-Based Gamma Sources

Although at first glance PuBe emits a monoenergetic gamma at 4.438 MeV, in reality it has a small distribution about this mean. A Geant4 simulation shown in Figure 3 reveals the expected energy distribution emitted from the $^{9}Be(\alpha, \gamma n)^{12}C$ based source.

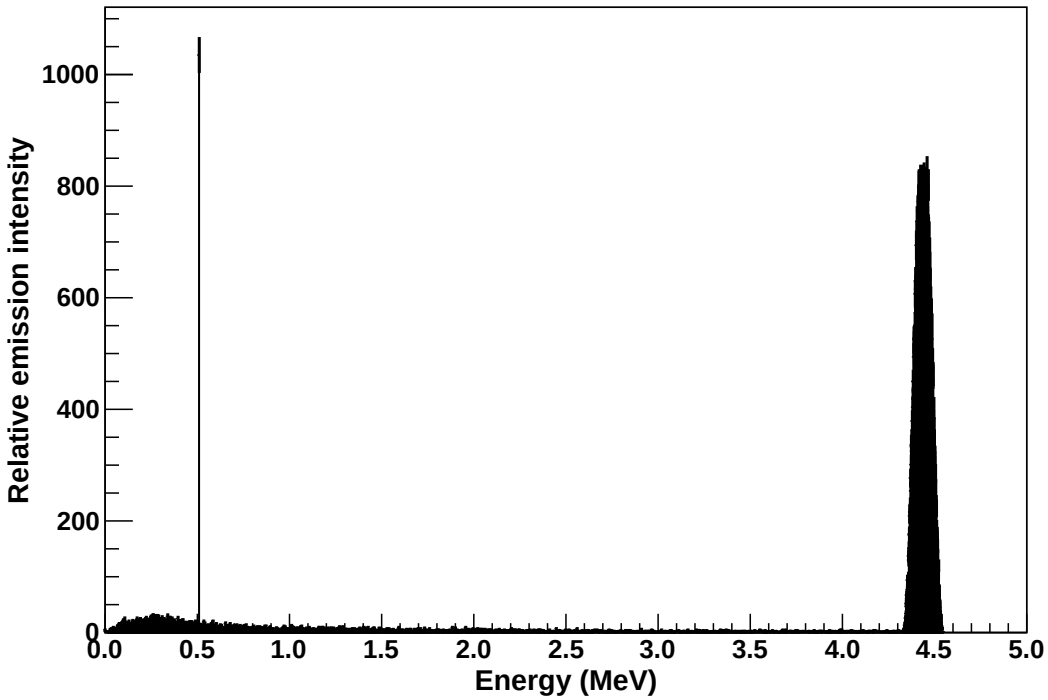

Figure 3: A uniformly distributed, monoenergetic, isotropic alpha source representing the alpha decay of plutonium is simulated in Geant4. This simulation accounts for the energy dependence of the alpha after some slowing down, the emission angle of the neutron, and the energy dependence of the carbon after some slowing down at the time of decay.

To determine the energy resolution of the detector at the energy of a broadened

gamma, we must quantify the gamma distribution from the reaction. Investigating ${}^{9}Be(\alpha,\gamma n)^{12}C$ as in PuBe, there are four phenomena that contribute to the gamma energy distribution. The first comes from the alpha slowing down in the medium, described by the Bethe formula for heavy charged particles, as in Eq. 7.

$$-\frac{dE}{dx} = k_C^2 \frac{4\pi n_e Z^2 e^4}{m_e v^2} ln\left[\frac{2m_e v^2}{I(1-\beta^2)} - \beta^2\right] \tag{7}$$

As long as the alpha maintains enough energy to induce the reaction, $E_\alpha \geq 1.264$ MeV [14], the alpha will be at some energy 1.264 MeV $\leq E_\alpha \leq$ 5.245 MeV when the reaction occurs.

After the reaction, the angle of emission of the neutron changes the available kinetic energy to the carbon. If the neutron is emitted 180° from the original momentum of the alpha, the carbon will have maximum energy.

This energetic carbon is also an excited state and will gamma decay to reach its ground state. The decay probability is a function of time, and as more time passes, the carbon slows down in the material, adding to the uncertainty of the carbon energy. The carbon at a given kinetic energy at the time of emission can also change the energy of the gamma depending on the angle of emission.

With the emission spectrum in Figure 3, we can extract the energy resolution by comparing a simulation with this gamma spectrum to the experimental data.

2.2.2 ${}^{11}_{5}\mathbf{B}({}^{2}_{1}\mathbf{H},\mathbf{n}\gamma){}^{12}_{6}\mathbf{C}$ Source and Measurement

The measurement used here was taken by P. B. Rose [18] at the MIT Bates Linear Accelerator Center. A cyclotron accelerates 3.02 MeV deuterons to a natural boron target to induce the reaction. As was the case for PuBe, this reaction-based source does not produce purely monoenergetic photons, but a broadened energy distribution about the emission energy. This reaction differs from PuBe in that it has a forward bias, whereas PuBe alpha particles are isotropically incident upon Be. Consequently,

the energy distribution is not symmetric, but is skewed toward higher energies, giving the unusual shape to the peaks in Figure 1.

Unfolding this spectrum is of particular interest because the relative yields of the gamma energies are not well known. The performance of the unfolding, however, is heavily dependent on the accuracy of the calibration.

The energy calibration was also performed in this work, using low energy check sources (below 3 MeV) and the well known 4.438 MeV and 15.1 MeV lines. The other gamma peaks between 4.5 MeV and 10 MeV potentially correspond to other transitions from the excited ^{12}C nucleus, shown in Figure 4. Purely from this kind of speculation, there seems to be two adjacent gamma energies in the 6 - 8 MeV region. However, the only transitions that could correspond are 7.45 MeV and 8.27 MeV, implying the calibration is slightly skewed to the left. If this 7.45 MeV transition occurs in ^{12}C, the 3.21 MeV transition should follow, though it is not clear it exists. The next peak corresponds well to the 9.64 MeV transition, but if it is also skewed to the left, could potentially come from the 10.67 MeV or even 12.70 MeV transitions.

Another explanation for these lines is neutron capture in surrounding elements such as Al, C, other isotopes of B, etc. These possibilities are not explored here due to their multitude.

Some work in characterizing this source is emerging due to the interest by the nonproliferation field. One work by Brandis et al [2] explores the 4.44 MeV and 15.1 MeV yields as a function of incident deuteron energy. The study indicates that at 3 MeV, the 4.44 MeV gamma was just over an order of magnitude higher in intensity than the 15.1 MeV gamma. This will serve as a point of comparison for the unfolding results.

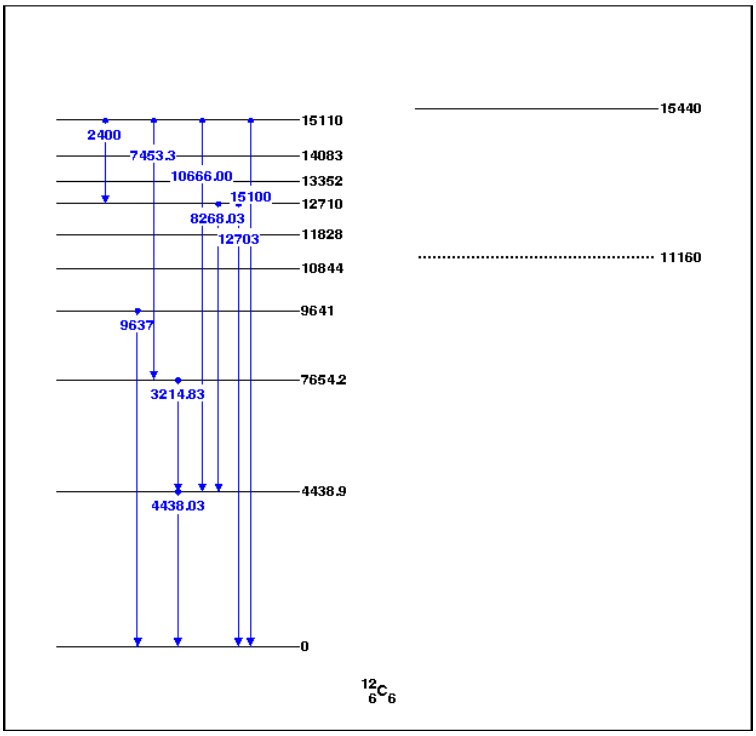

Figure 4: The excited nuclear states and possible transitions are shown from ENSDF [3].

CHAPTER III

DEVELOPMENT OF COMPUTATIONAL METHOD

The general methodology for unfolding, outlined in Figure 5, is a semi-analytic iterative matrix-unfolding approach. It uses the combined results of experimental data and simulation to create a response function matrix. This matrix is then used for the decomposition of known and unknown gamma spectra.

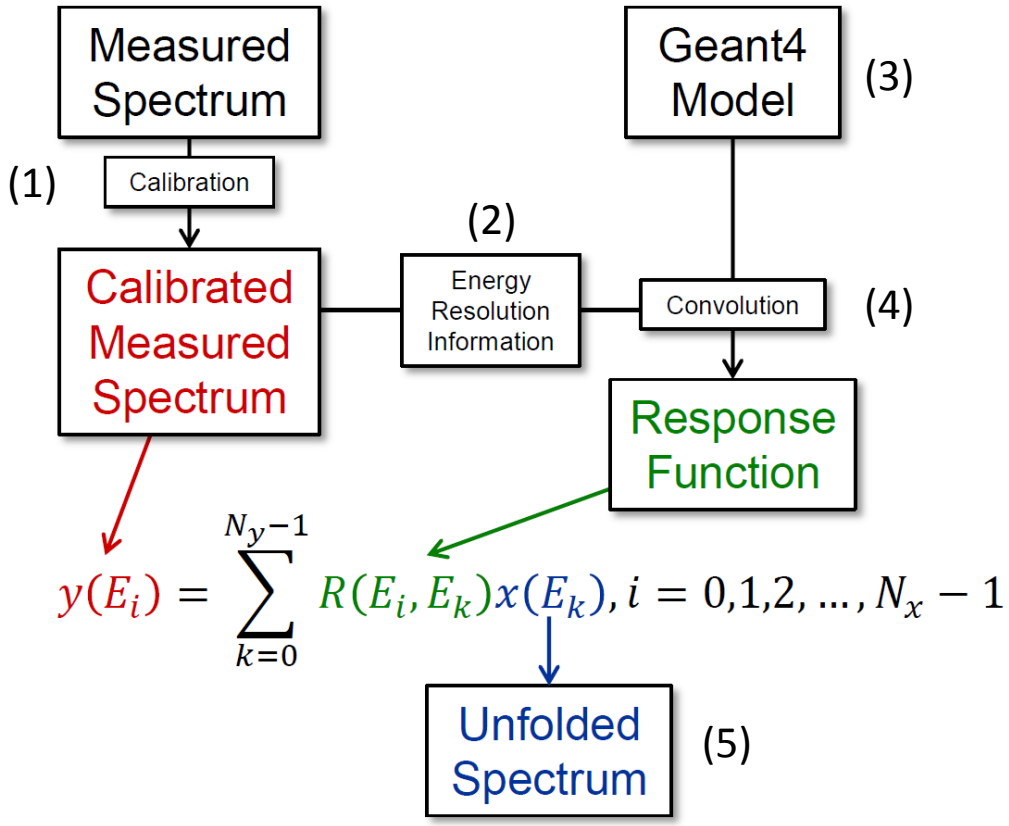

Figure 5: The implementation details of the method include the particular inputs and outputs. Experimentally measured spectra are used for two purposes: to extract energy resolution information and to be unfolded. The simulation generates an ideal energy deposition matrix that requires the energy resolution information to match experimental results. Finally, deconvolving the experimental spectrum with the response matrix outputs the unfolded spectrum.

The diagram takes two input types, measured spectra and a Geant4 model. The first step in the process is to energy calibrate the experimental spectra (1), as discussed in Section 2.2. The experimental spectra can then be related to the Geant4 simulation which models energy deposition. Also from the experimental spectra, the energy resolution information for the detector of interest is extracted (2), discussed in Section 3.2. This will be incorporated with the simulation to have a more accurate representation of the detector response function.

Next, the Geant4 model is made (3), simulating the energy deposition in $LaBr_3$(Ce) over a range of photon energies. This represents the an ideal detector response with perfect energy resolution. Next, the simulation results are combined with the experimental energy resolution via convolution (4). Now, the response function can be used to deconvolve the incident photon spectrum from an experimentally measured spectrum from its detector response (5) using the deconvolution algorithm described in Section 2.1.2.

3.1 Creating the Response Function Matrix in Geant4

The matrix-unfolding method intrinsically requires a response function matrix that represents the detector response from photons that span the energy range of interest. The physics code Geant4 is capable of synthesizing this matrix by simulating the transport of radiation through matter. Geant4 is first used to calculate the energy deposition distribution in a $LaBr_3$(Ce) crystal without regard to the later processes such as scintillation, PMT multiplication, or subsequent electronics. Post-processing of the response function accounts for the statistical fluctuations of these downstream steps.

The model contains a cylindrical $LaBr_3$(Ce) crystal 1.5"-length and 1.5"-diameter suspended in a detailed model of the Georgia Tech neutron generator vault. The photon beam is a monoenergetic, isotropic point source and is 100 cm from the center

of the detector. One assumption is the source is not self attenuating, i.e. the source is sampled from a point in air, not from within the respective material. Additionally, it assumes that the radiations are independent in time and there is no possibility of coincidence.

The response function is created for gamma energies up to 6 MeV, consisting of 1200 energies. Each event randomly sampled from this subset of energies and recorded the energy deposition in the detector in a two-dimensional histogram. The energies span 0.005 MeV to 6 MeV with 5 keV intervals. Figure 6a shows a sample energy spectrum from a sub-simulation with incident photon energy at 2 MeV.

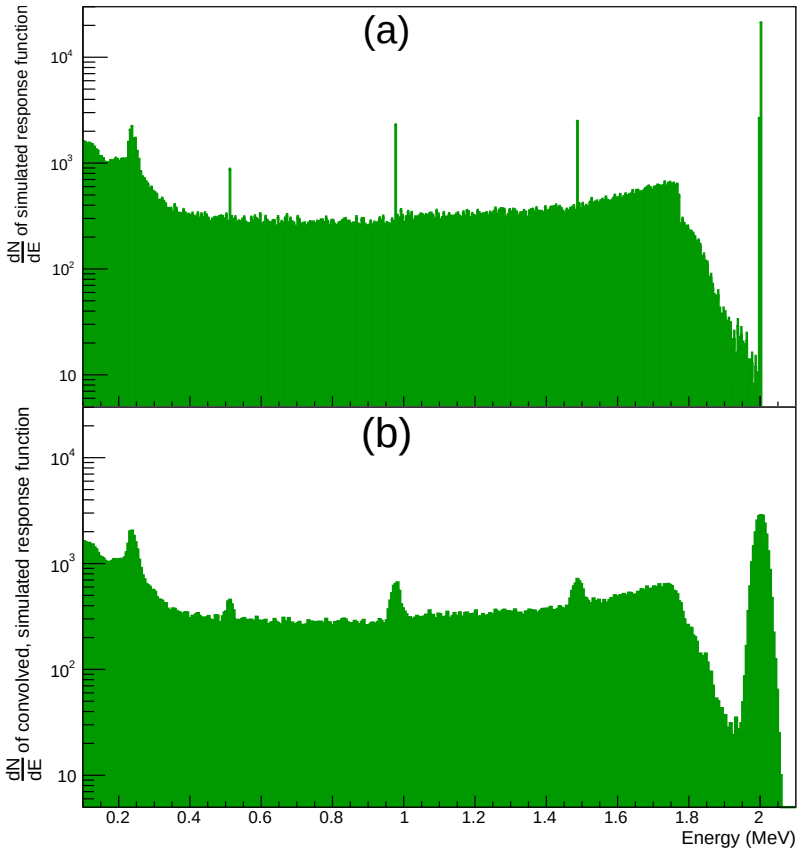

Figure 6: An example simulated spectrum (a) at 2 MeV represents the frequency of energy deposition for each energy bin in $LaBr_3(Ce)$. The simulation, however, does not account for the scintillation or signal amplification processes. In (b), the spectrum is convolved with empirical energy resolution information to better represent the detector response.

3.2 Accounting for Energy Resolution

The synthesized response function from Geant4 is a calculation of the energy deposition in the detector by charged particles per incident photon. The model generating the response function is an oversimplification of the physical processes that take place in a scintillator. This is a necessary simplification because of the high light output in a $LaBr_3$(Ce) crystal, with about 63,000 scintillation photons per MeV deposited in the detector [9]. Modeling the scintillation response for each incident photon is impractical, both for computational considerations and the accuracy of optical parameters needed; so another method to account for the realistic detector response is employed. The check sources used for energy calibration provide this additional energy resolution information.

3.2.1 Extracting Empirical Energy Resolution

The energy resolution from experimental spectra provide the necessary information to empirically spread the energy deposition responses created in the Geant4 model. Assuming that a peak can be estimated as a Gaussian, the $\frac{FWHM}{H_0}$ of each calibration peak is plotted against the corresponding mean energy H_0 of that Gaussian, shown in Figure 7.

The fitting function, Eq. 8, is used to model the energy resolution where α and β are particular to the scintillator and PMT, R is the fractional energy resolution, and H_0 is the mean energy [11]. The $\frac{1}{\sqrt{E}}$ dependency reflects the notion that the scintillation counting is governed by Poisson counting statistics.

$$R = \frac{FWHM}{H_0} = \frac{\sqrt{\alpha + \beta E}}{E} \tag{8}$$

As mentioned in Section 2.2.1, the method for calculating the energy resolution for the 4.438 MeV gamma from PuBe includes calculating the theoretical gamma distribution via Monte Carlo simulation. The energy resolution is the deconvolution

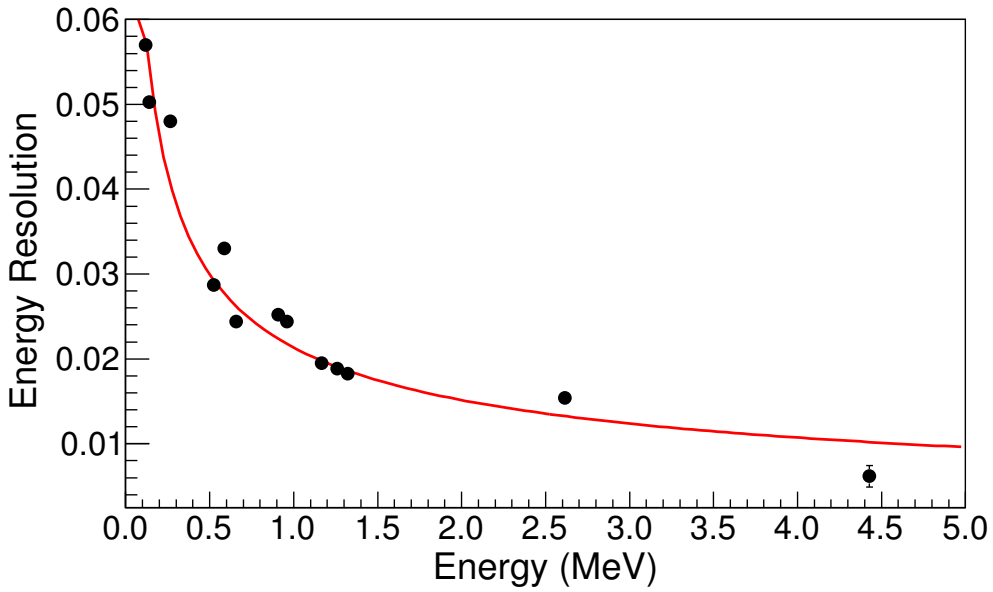

Figure 7: The energy resolution information is taken from experimental data from ^{22}Na, ^{137}Cs, ^{60}Co, a mixed thorium source, and PuBe. The energy resolution for the PuBe peak is extracted by deconvolving the experimental peak with the calculated theoretical peak width.

of the theoretical distribution from the measured one. This is done iteratively by finding the Gaussian spreading function that minimizes the L^2-norm of the residual. Figure 8 (right) shows the Gaussian spread simulation, $f(E)$ for a variety of sigma values. Each of these $f(E)$ is then compared to the experimental spectrum, $g(E)$. The L^2-norm of the difference is then calculated for each sigma value. For a the two discrete functions, this norm is defined as

$$error = \sqrt{\sum_{i=0}^{N-1} (f(E_i) - g(E_i))^2} \tag{9}$$

Figure 8 (left) shows this error as a function of sigma. Choosing the sigma that minimizes the error, we now have the energy resolution needed to spread the theoretical PuBe spectrum to match the experimental spectrum. The corresponding result of the sigma with minimum error is highlighted in Figure 8 (right).

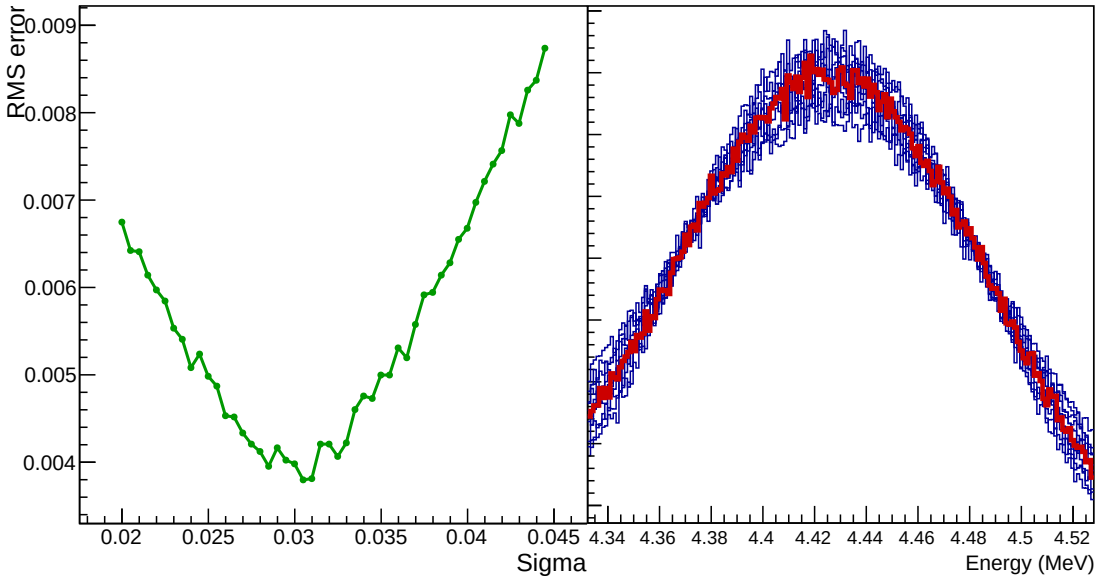

Figure 8: To determine LaBr's energy resolution at 4.438 MeV, the theoretical gamma distribution that PuBe emits is spread with varying sigma values. We then choose the sigma value that minimizes the error between this function and the experimental spectrum.

3.2.2 Convolution of the Response Function Matrix

The response function uses the energy resolution information to match the actual response of the detector. This first requires an assumption that each impulse can be spread as a Gaussian with a standard deviation $\sigma(E)$ where

$$\sigma \approx \frac{FWHM}{2.3548} \tag{10}$$

is evaluated from the fitting function in Figure 7 at the mean energy of the incident energy. Thus, the standard deviation is constant for each Gaussian function evaluation in Eq. 11.

$$f(E,\mu) = \frac{1}{\sigma(\mu)\sqrt{2\pi}} e^{-(E-\mu)^2/2\sigma(\mu)^2} \tag{11}$$

The convolution process is described by Eq. 12.

$$R'(E_i, E_k) = \sum_{l=0}^{N-1} f(E_i, \mu = E_l) R(E_l, E_k) w, i = 0, ..., N-1, k = 0, ..., M-1 \quad (12)$$

This matrix multiplication creates the Gaussian spread response function. However, the approach taken for creating the response function is stochastic. For a given response (from a single incident energy), a given energy bin is Gaussian spread stochastically. For a bin with N counts, a value is sampled from a Gaussian centered at that bin with standard deviation dictated by the energy resolution curve, Eq 8.

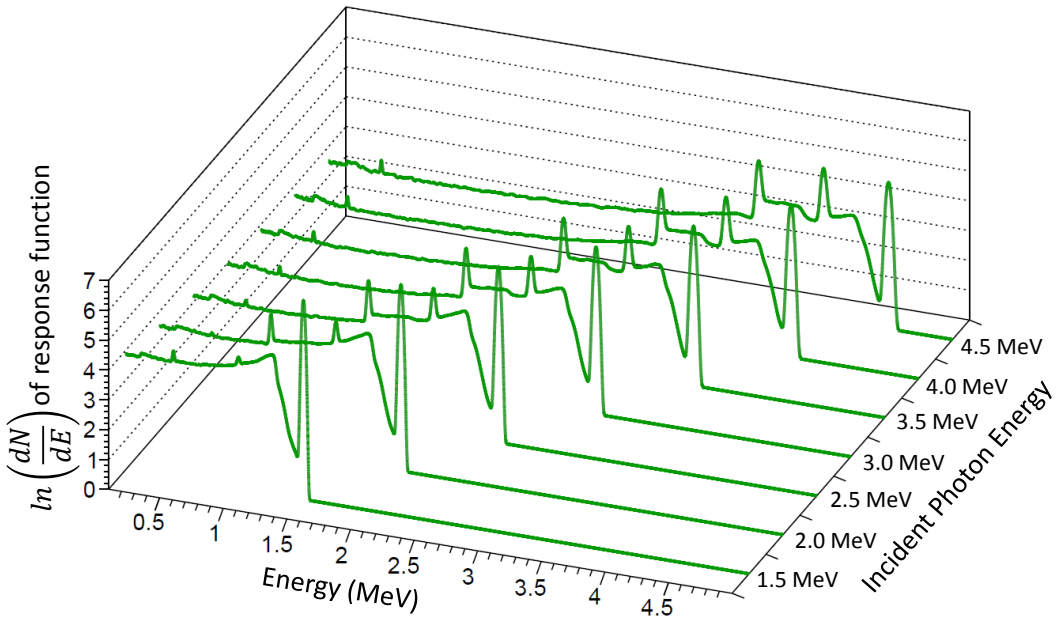

Figure 9: After convolution, the total response function matrix represents how the detector will respond to different incident gamma energies. This example shows a subset of 9 energies out of the $\sim$ 1000 energies in the full matrices.

The motivation behind using a stochastic approach to spreading the function is that the response function maintains integer counts in each bin. This more clearly maintains Poisson statistics.

3.3 Unfolding a Spectrum

After calibrating the experimental spectrum, generating the response function and convolving the response function, the Gold decomposition algorithm is used to solve

Eq. 3. ROOT already contains an implementation of this algorithm which is used for the unfolding. With the experimental spectrum, the response function, the sizes, number of repetitions, and a boosting parameter, the code generates the unfolded spectrum.

It is also of interest to determine what the error is on the unfolded spectrum. The unfolded spectrum will have error due to the existence of statistical error in the measured spectrum (input vector). In a paper by R. Gold and E. F. Bennett [6], they found that the error associated with iteratively unfolding $y = \mathbf{R}x$ is described by

$$S_y = \mathbf{B}S_x \tag{13}$$

where the elements of the vector S_y are the variances $\{\langle(\delta y_i)^2\rangle\}$ and the elements of S_x are $\{\langle(\delta x_i)^2\rangle\}$. The matrix B has elements $b_{ij} = (r_{ij})^2$ for $i, j = 1, 2, ...n$. This result can be achieved assuming that error in the response function is small relative to that of the measured spectrum. Essentially, this is a second unfolding problem similar to the original problem.

CHAPTER IV

EVALUATION OF COMPUTATIONAL METHOD

4.1 Evaluating the Quality of the Response Function

The response function matrix is created by first simulating energy deposition in the detector, then spreading the spectrum using empirical data. Before the response function is used for unfolding, it is important to check the accuracy of the model used to generate the response function. To do this, we simulate the decay of ^{60}Co: two independent, isotropic gammas. The first gamma at 1.3325 MeV happens 100% of the time, and the other at 1.1732 MeV occurs 99.88 % of the time.

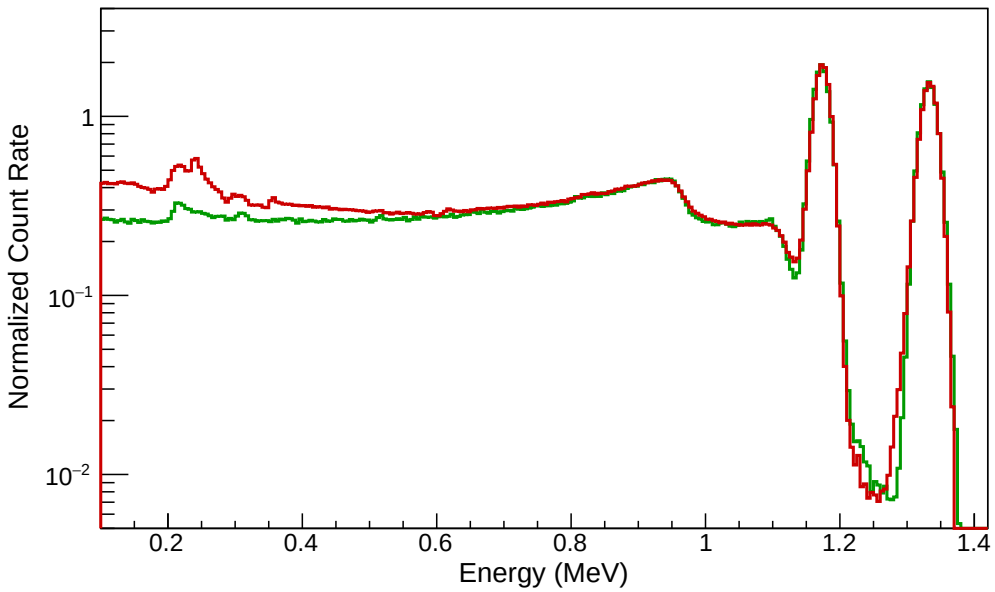

Figure 10: A comparison of the model (green) and experiment (red) for the ^{60}Co transitions demonstrates the quality of the model. The model is scaled such that the 1.33 MeV peak has the same magnitude in both.

The results of the simulation (green) and the experimental spectrum (red) are plotted together in Figure 10. Several features align well, including the Compton

edges and the photopeaks. There are, however, discrepancies between the spectra, in particular the low energy side of the Compton continuum. Qualitatively, it is clear that the model underestimates certain aspects of the low energy gammas. One potential reason are that the room return is not modeled accurately. However, the room is modeled in great detail, so it is not the lack of some geometric features. If this is the reason, it implies that Geant4 inaccurately models gammas at low energies. Geant4, however, is a well-validated code, especially for gamma and electromagnetic interactions. Another potential source of error is the lack of PMT and physical source modeling, i.e. the source is modeled as a point with no material.

To test this discrepancy, a PMT and source material are added independently to the model. The addition of the PMT showed little to no change in the response. However, the addition of source material dramatically increased the low energy region, showing significantly better agreement with experiment. This, however, is impractical to account for when generating the full response function. Because the various sources used have different material properties, a more general material-less response function is used with the understanding that it will always introduce low-energy error.

In addition to a qualitative explanation for the features, the spectral differences can be quantified by comparing several parameters: total efficiency, peak efficiency, and peak-to-Compton ratio. These results for ^{60}Co, listed in Table 4.1, show that when comparing features to either the total number of counts (peak-to-total) or to number of source particles (total and peak efficiency), the simulation under estimates the parameters. This can be attributed to the same source of error as the back-scatter error as discussed before: the simulation under estimates total number of counts relative to the peak/number of emitted particles. The response function is in good agreement for the peak-to-Compton ratio for both peaks, showing that the interaction probabilities for a gamma with full energy in the detector is well-predicted in the model.

Table 1: Comparison of spectral features between an experimental and simulated ^{60}Co spectrum

Peak Energy	Parameter	Experiment	Simulation	% error
-	Total Efficiency	$2.205 * 10^{-2}$	$1.346 * 10^{-2}$	63.82 %
1.1732 MeV	Peak Efficiency	$1.346 * 10^{-5}$	$0.997 * 10^{-5}$	35.01 %
	Peak-to-Total	$6.181 * 10^{-4}$	$7.406 * 10^{-4}$	16.54 %
	Peak-to-Compton	0.2334	0.2301	1.43 %
1.3325 MeV	Peak Efficiency	$1.070 * 10^{-5}$	$0.830 * 10^{-5}$	28.92 %
	Peak-to-Total	$4.854 * 10^{-4}$	$6.167 * 10^{-4}$	21.29 %
	Peak-to-Compton	0.1858	0.1717	8.21 %

This comparison works well for gamma energies below 2 MeV where pair production is not prominent, but it is also of interest to investigate the peak-to-single-escape and peak-to-double-escape ratios. To do this, we simulate the gamma spectrum of PuBe as was done to calculate the energy resolution in Section 3.2.1. The simulation (green) and experiment (red) are shown together in Figure 11. To simulate PuBe, only the gamma produced in the (α, n) reaction is considered. The emission spectrum, shown in Figure 3, is the same as the one used to determine the energy resolution at 4.438 MeV.

A superficial inspection reveals several discrepancies between the two spectra. Further consideration of the source used, however, helps explain some of these differences. First, PuBe does emit a 4.438 MeV gamma, but also contains a significant amount of ^{239}Pu and other actinides that have accumulated. These isotopes typically have low energy gamma emission, explaining the peaks present in the experimental spectrum at lower energies. Additionally, this 1 Ci plutonium source has high activity and is prone to causing pile-up in the detector. This causes a significant increase in counts

in the Compton region of the 4.438 MeV peak. Further, because PuBe is a gamma and neutron source, it is expected that neutrons in the room will induce (n, γ) reactions, increasing the number of gammas present. For example, there is a visible 2.2 MeV gamma in the experimental spectrum that is not accounted for in the simplified model.

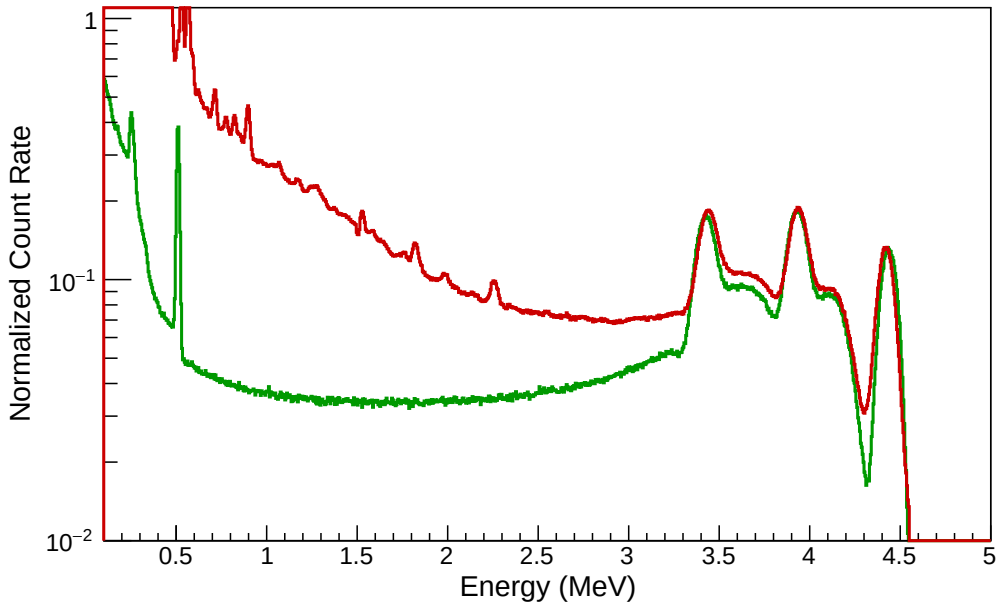

Figure 11: A comparison of the model (green) and experiment (red) for PuBe's 4.438 MeV demonstrates the quality of the model. The model is scaled such that the 1.33 MeV peak has the same magnitude in both.

Limiting the investigation to the low energy features of the spectra, we instead look to the single escape peak (SEP) and double escape peak (DEP). Exploring anything else would only be useful if PuBe were modeled in its entirety, both neutron and low energy gamma emission. The relative height of the escape peaks to the full-energy deposition peak are listed in Table 4.1. Similar to the peak-to-Compton ratio for ^{60}Co, these peak-to-SEP and peak-to-DEP ratios are in good agreement between experiment and simulation. We can thus expect the unfolding algorithm to unfold even higher energy photons that produce SEPs and DEPs.

Table 2: Comparison of escape peaks between an experimental and simulated PuBe spectrum

Parameter	Experiment	Simulation	% error
Peak-to-SEP	1.425	1.389	2.53 %
Peak-to-DEP	1.391	1.330	4.39%

This evaluation of the model indicates that the unfolding algorithm using this model for the response function will generate reasonable results. We expect that in the low energy region, the unfolding code will predict additional gamma lines that represent in-scatter that is not accounted for in the model. Additionally, any pile-up from a high activity source or a neutron source like PuBe will be seen as gamma lines that are not directly from the source but are seen by the detector. Figure 12 shows the final response function.

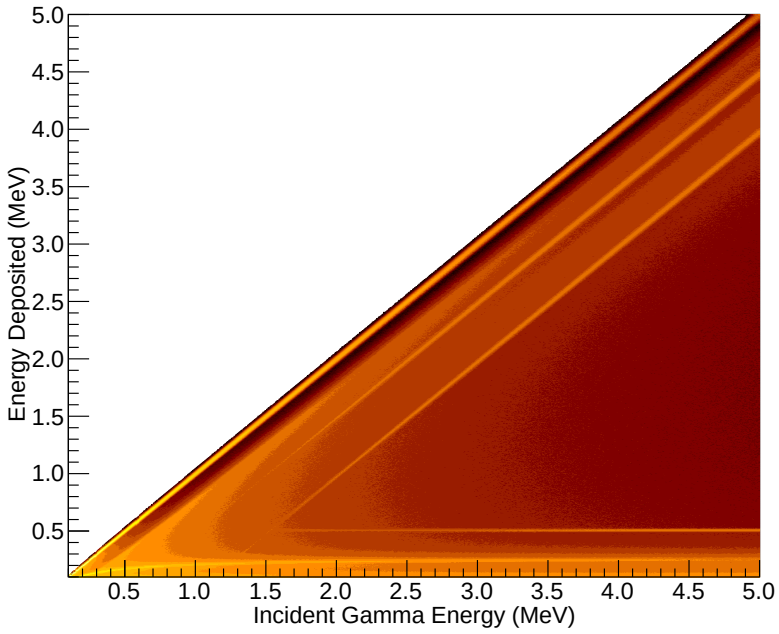

Figure 12: Final response function used for unfolding.

4.2 Exploring the Unfolding Parameters

As discussed in Section 2.1.2, Gold's decomposition algorithm is used to solve x in the original $y = \mathbf{R}x$ equation. This algorithm uses an iterative approach, with three input parameters that constrain the algorithm: number of iterations, number of repetitions, and boosting factor. The number of iterations is the most straightforward. A solution $x = [1, 1, ..., 1]^T$ is first guessed, then is updated as

$$x_i^{(k+1)} = x_i^{(k)} + \frac{x_i^{(k)}}{\sum_{m=0}^{N-1} \mathbf{A}_{im} x_m^{(k)}} \left[z_i - \sum_{m=0}^{N-1} \mathbf{A}_{im} x_m^{(k)} \right] \tag{14}$$

This is repeated for the number of iterations, L, specified. This x converges to some positive-definite vector after some number of iterations past which more iterations has no effect.

The boosting factor, p, and number of repetitions, R, are related parameters. If $p > 1$, then once the algorithm has finished L iterations, it boosts the vector x as $x_i^{(0)} = \left| x_i^{(L)} \right|^p$. Then, the iterative process in Eq. 14 performed again with L iterations. This overall boosting process is repeated R times.

It is not immediately clear which combination of these three parameters will yield the best performance of the algorithm. To gain insight, a small study is done on the ^{60}Co spectrum. Holding the boosting factor p constant, the spectrum is unfolded, then the RMS error is calculated from $||Rx - y||_2$ for an increasing number of repetitions and iterations. Each case is also compared against $p = 1$, no boosting. The results with boosting factors $p = 2, 3, 4$, and 5 are shown in Figure 13. These results show that using some boosting consistently performs better than no boosting. However, neither change in the boosting factor nor the number of repetitions shows significantly different performance. Thus, the conclusion for choosing the parameters is to first choose $p = 2$, $R = 2$, because these take the least time to compute. Then, increase the iterations until a consistent minimum is achieved. In the case of ^{60}Co, this minimum occurs at 6000 iterations with RMS of 0.06289.

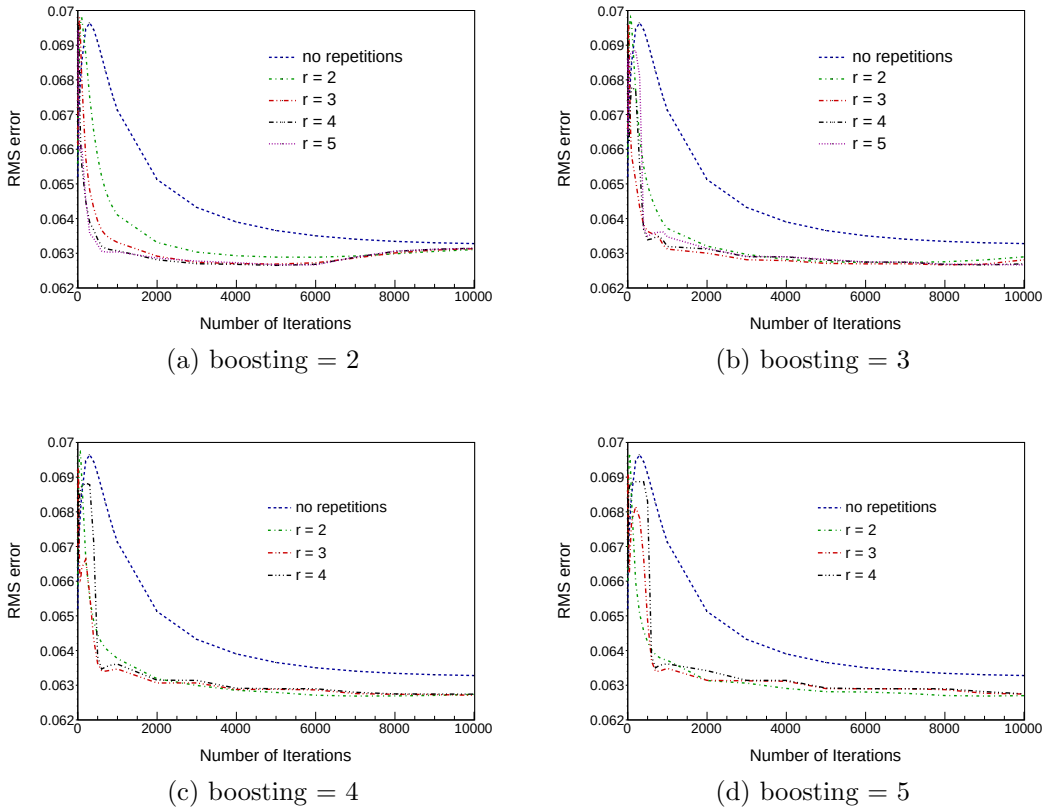

(a) boosting = 2 (b) boosting = 3

(c) boosting = 4 (d) boosting = 5

Figure 13: A comparison of the unfolding parameters shows that boosting improves the performance, but the other parameters play little role in the accuracy of the unfolding.

This argument works well for spectra with defined peaks, but breaks down when the spectrum is more continuous. In unfolding applications, these typically come in two varieties. First, there are spectra with few to no peaks, such as a fission or bremsstrahlung spectrum. These are not explored in this work, but it is speculated that the algorithm will perform best with no boosting, as the role of the boosting is to strengthen the peak height. Second, there is the case where there is some spreading about a mean gamma energy, such as in PuBe. The unfolding is expected to yield the total number of counts proportional to the integral of that peak (off by the efficiency of the detector). The boosting allows the peak height to be amplified, and the peak spreading effect from the reaction kinematics is subdued.

This would suggest that this algorithm's purpose is to predict the number of

gammas needed to produce a spectrum and what mean energies those gammas had. In the case of a broadened peak, the unfolding should not reproduce the original incident distribution, but an impulse at its mean energy. To unfold a continuous spectrum, either no boosting should be applied, or a different algorithm should be used.

4.3 The Unfolded Spectra

4.3.1 ^{137}Cs, ^{22}Na, and ^{60}Co

Using the parameter selection process discussed in Section 4.2, Gold's decomposition is applied to ^{137}Cs, ^{60}Co, and ^{22}Na spectra. In order to better highlight the features of the unfolded spectra, they are plotted in semi-log.

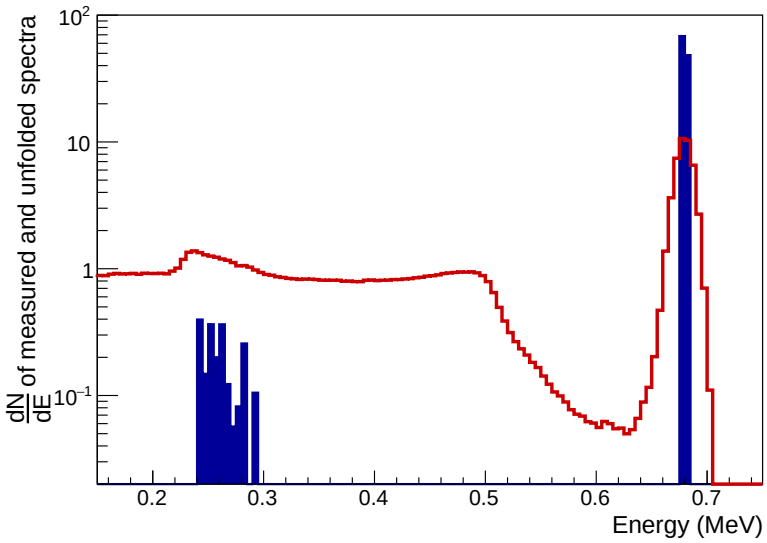

Figure 14: Semi-log plot of the measured (red) and unfolded (blue) ^{137}Cs spectra.

The ^{137}Cs measured and unfolded spectra are shown in Figure 14. The unfolded spectrum (blue) shows a sharp peak at the center of the measured spectrum's photopeak. Its relative height to the photopeak is understated in the semi-log plot, but it is nearly an order of magnitude higher, which is to be expected for several reasons. The response function accounts for total efficiency and for events that resulted in

Compton scatter in the detector. The height of this peak should correspond do the total number of *incident* photons of that energy.

The unfolded spectrum also has additional low energy counts. The analysis of the response function quality revealed discrepancies between measurement and model at low energies, particularly surrounding the backscatter peak. The model under-predicted the low-energy region, meaning the unfolded spectrum requires additional counts in this region to account for the perceived elevated number of counts in the measured spectrum. This phenomenon occurs in all unfolded spectra and will only be mentioned here for brevity.

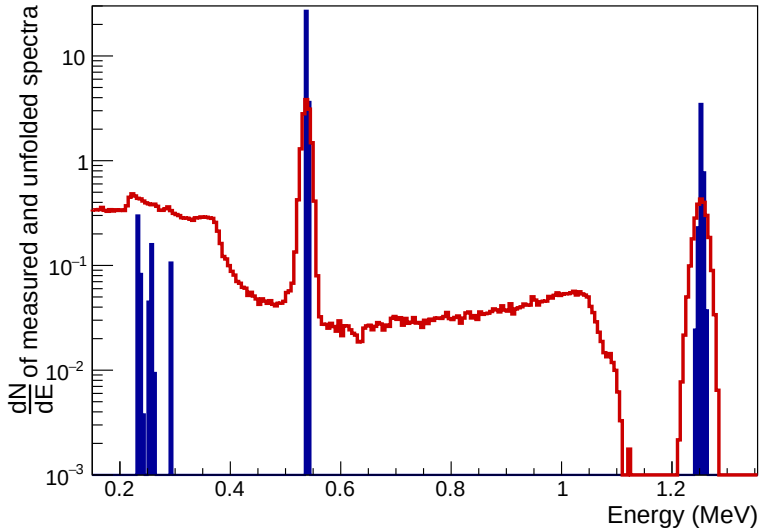

Figure 15: Semi-log plot of the measured (red) and unfolded (blue) ^{22}Na spectra.

Similar results are found when applying the algorithm to ^{22}Na. Shown in Figure 15, the decomposition algorithm shows peaks corresponding to the 1.275 MeV and 0.511 MeV peaks emitted from the source. The unfolded 1.275 MeV peak is not quite an impulse – this phenomenon is discussed further in the ^{60}Co analysis.

The next spectrum, ^{60}Co, shown in Figure 16, has two peaks at both photopeaks. These peaks, however, are not sharp impulses as expected for a monoenergetic gamma source. Rather, there is a small spread around each photopeak, the reason for which

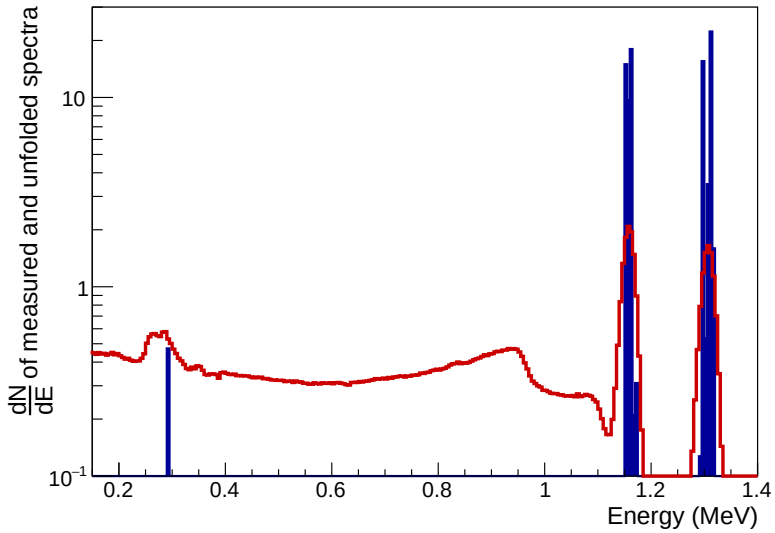

Figure 16: Semi-log plot of the measured (red) and unfolded (blue) ^{60}Co spectra.

is not immediately clear. A possible explanation is that the Gaussian spreading fit, shown in Figure 7, is not perfect. Additionally, it could likely be an artifact from the decomposition algorithm and could be suppressed with a more careful selection of the parameters. As mentioned in Section 4.2, the parameters boosting parameters are both 2, and the number of iterations was chosen by finding the minimum 2-norm of the residual (in this case 4000). This was the selected approach because increasing the number of repetitions and the boosting factor did not decrease the residual norm much past 2. However, using a boosting factor of 10, 10 repetitions, and 10000 iterations, the results are seemingly more physical, shown in Figure 17. Although the spread is not completely reconciled, this plot does not nearly have the spread as Figure 16.

Although this intuitively seems more physical, it is useful to quantify the accuracies of each in some way. To do this, the ratio of the total counts in each peak is calculated and compared to the ^{60}Co decay scheme. For the unfolded spectrum calculated using the parameters 2, 2, 4000, the ratio is 0.9895, and for that using 10, 10, 10000, the ratio is 0.9635. Both results are close to the theoretical result, 0.9988, within 3.5%. The first unfolded spectrum with lower parameters yields the slightly

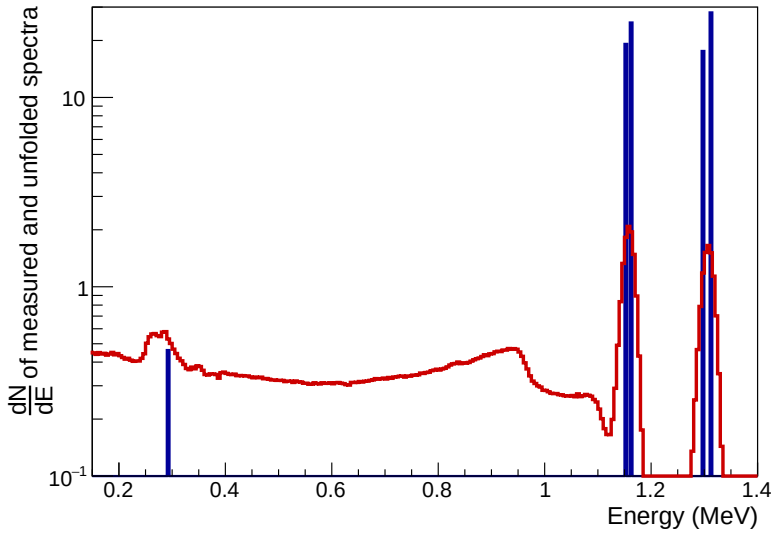

Figure 17: Semilog plot of the measured (red) and unfolded (blue) ^{60}Co spectra.

better ratio with 0.93 % error.

This does raise the question of whether this approach for choosing the parameters is the best. Some alternative options are proposed in Section 5.

4.3.2 PuBe

In addition to the check sources used in the previous section, the unfolding method was designed to unfold up to 5 MeV beams, including the gamma spectrum from PuBe. This task is more challenging, however, because the gammas that are emitted are not discrete at 4.44 MeV. Instead, there is a broadening about this energy, discussed in detail in Section 2.2.1.

Using the previous method, the first step is to determine the 2-norm of the residual for increasing iterations, with boosing factor as 2 and the number of repetitions as 2. Using this approach, the resulting unfolded spectrum is shown in Figure 18 with 8000 iterations. These results look far different from those of the check sources, not only because of the continuous nature of the incident energy distribution, but because of the prominence of the single and double escape peaks.

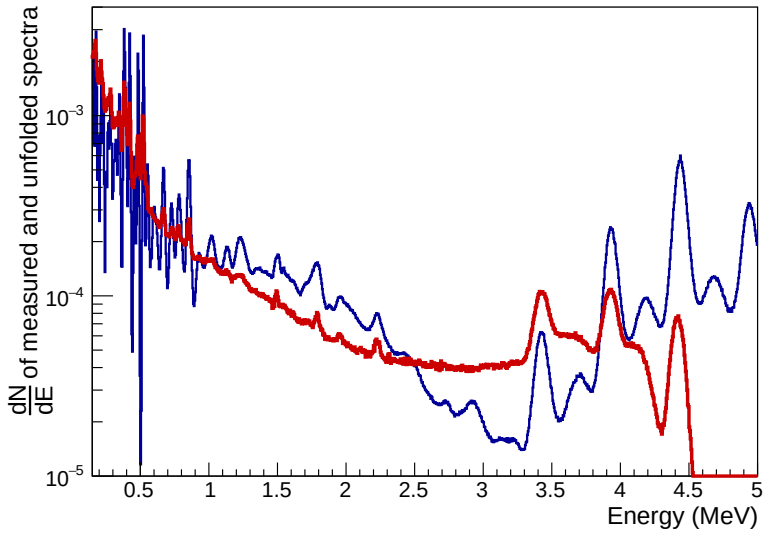

Figure 18: Semi-log plot of the measured (red) and unfolded (blue) PuBe spectra with 8000 iterations, 2 repetitions, and boosting of 2.

The algorithm has the challenge in this case to discriminate full-energy peaks from the escape peaks, making this spectrum more ill-conditioned than the previous spectra. The typical structure for a monoenergetic spectrum has a full-energy peak with two escape peaks to the left, each 0.511 MeV than the previous peak. When attempting to unfolded, considering the single-escape peak (in this case at 3.93 MeV) as a possible full-energy peak, there is both a peak at full-energy and one 0.511 MeV to the left. Although it does not completely fit the three peak structure, it does satisfy two of those peaks. Similarly, in the case of 0.511 MeV above the full-energy peak at 4.95 MeV, there are two peaks to the left that account for two of the three peaks expected for a gamma at this energy. These two cases, 3.93 MeV and 4.95 MeV, are less prominent than the true energy of 4.44 MeV because they do not satisfy but two of the three peaks. Further, at 1.022 MeV lower (3.42 MeV) and likely at 1.022 MeV higher (5.46 MeV), an even smaller peak is shown, because it only satisfies one of the three peaks necessary.

In attempt to achieve a single energy in the unfolded spectrum at 4.44 MeV, the

parameters are pushed (as was done for ^{60}Co) to 10^4 iterations, 10 repetitions, and a boosting of 10. These are chosen empirically, such that beyond them, there is little to no change in the resulting unfolded spectrum. Using the 2-norm of the residual as the measure of error, the error for the lower parameters ($2.809*10^{-3}$) is only marginally lower than that for the higher parameters ($2.945*10^{-3}$). As shown in Figure 19, there is now a large line at 4.44 MeV, three between 1 and 2 MeV, and several below 1 MeV.

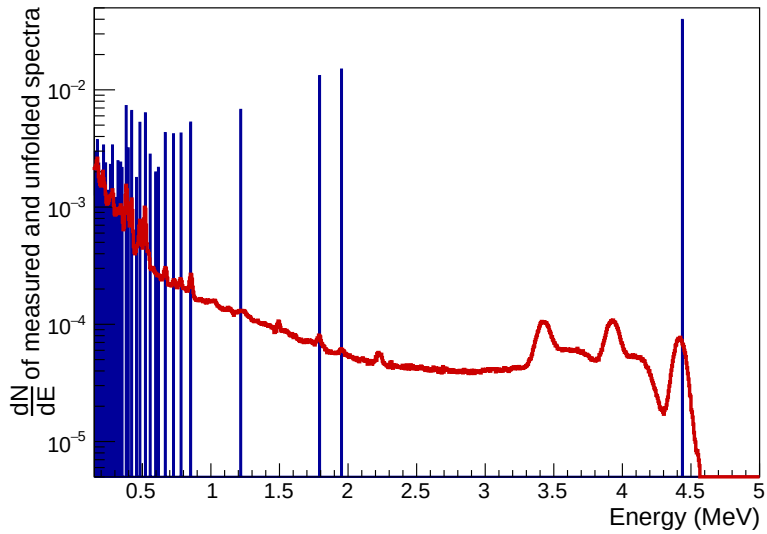

Figure 19: Semi-log plot of the measured (red) and unfolded (blue) PuBe spectra with 10^4 iterations, 10 repetitions, and a boosting of 10.

As in the case for the unfolded spectrum with lower parameters, there are several peaks below 1 MeV. Though here, the peaks are much more finely resolved. These peaks are understood to be the low energy gammas emitted by plutonium and the other actinides present in the PuBe source. The accuracy of these lines is not examined here.

The peaks between 1 and 2 MeV are likely products of discrepancy in the model and reality. This discrepancy is actually twofold. First, the high intensity of the source induces more pileup in the detector where none is accounted for in the model. Second,

the presence of neutrons in the room can induce (n, γ) reactions in the room, creating additional noise and peaks in the spectrum. In particular, the gamma produced in hydrogen neutron capture at 2.2 MeV and its corresponding escape peaks are not properly recognized. Because the response function does not account for the extra scatter in the room and because the algorithm is geared toward peak amplification, these small SNR peaks are either missed or mislabeled.

This use of higher valued parameters comes at the cost of losing the distribution of about 4.44 MeV, only highlighting the importance of properly choosing the parameters. For more continuous spectra, lower parameters seem to maintain this nature more effectively. For discrete spectra, higher parameters seem to perform better. This is intuitive when revisiting the purpose of each parameter. The number of iterations is purely for convergence, but the boosting and repetitions apply nonlinear transformations, amplifying higher values relative to the lower ones. This in particular is useful for a space like this where peaks contain the majority of the desired information.

4.3.3 Low-Energy Reaction Beam

To unfold the LENR beam, a modified version of the approach is applied. First, the model used to create the response function is simplified because the facility information is unavailable. Instead, a planar beam is perpendicularly incident upon the detector volume, which is suspended in air. Additionally, there is no energy resolution information available at energies beyond 4.438 MeV, so the fitting function is simply evaluated up to the necessary energies to approximate the response function. The unfolding parameters are heuristically chosen to maximize peak sharpness, 10^4 iterations, 10 repetitions, and a boosting of 10.

Despite the crude model and energy resolution approximations, the results show gamma lines in nearly all the places expected, shown in Figure 20. The particular

energies of interest (those 3 MeV and above), have the energies and intensities described in Table 4.3.3. To better show the relative intensities, Figure 20b is shown with a semi-log measured spectrum and a scaled, linear unfolded spectrum.

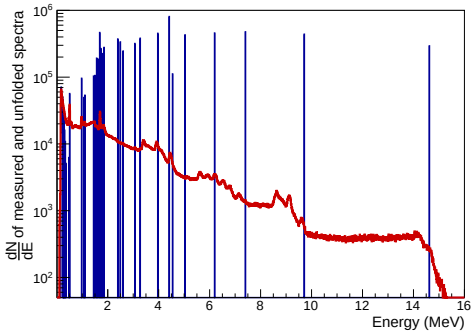

(a) both measured and unfolded in semi-log

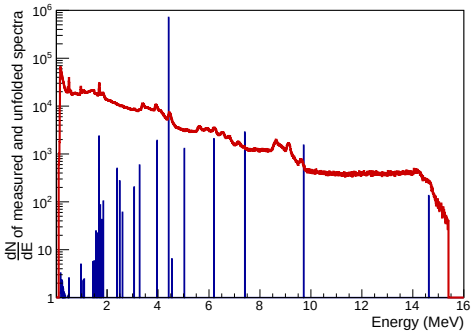

(b) measured in semi-log, unfolded in linear

Figure 20: The two plots show the measured and unfolded spectra for the LENR gamma distribution in different scales.

Table 3: Energies and intensities of unfolded gamma lines relative to maximum

Energy (MeV)	Relative Intensity
3.065	39.48 %
3.275	47.32 %
3.965	56.08 %
4.415	100 %
4.545	13.84 %
5.035	53.20 %
6.195	56.71 %
7.405	59.08 %
9.715	54.41 %
14.625	36.39 %

As was predicted by the available ^{12}C transitions, the 3.065 MeV and 3.275 MeV peaks neighbor the 3.21 MeV transition that is necessary if a 7.45 MeV occurs. The 6.195 MeV line has no corresponding transition in ^{12}C, indicating it either comes from some other reaction or is a mis-calibrated 7.45 MeV transition. If this is the case, the nearby 7.405 MeV line would shift to the right, possibly to where a 8.27 MeV transition would lie. This would also likely push the 9.715 MeV to the right, possibly to the 10.67 MeV transition. An alternative explanation is the 6.195 MeV results from another reaction, the 7.405 MeV corresponds to the 7.45 MeV transition, and the 9.715 MeV to the 9.64 MeV transition. A more detailed calibration would provide more insight into these discrepancies.

The two transitions typically of interest are 4.44 MeV and 15.1 MeV. If only the 4.415 MeV line corresponds to the 4.44 MeV transition and the 14.625 MeV to the 15.1 MeV, the 4.44 MeV intensity is only larger by a factor of 2.75. This is much smaller than the predicted order of magnitude in [2] for 3 MeV deuterons. It is likely that given the crudeness of the model, the peaks surrounding 4.44 MeV also correspond to this transition. After applying this correction, the 4.44 MeV peak is 6.13 times larger than the 15.1, still smaller than the published ratio, possibly due to the over-simplification of the model.

Finally, of small consequence but of notice is the underestimation of the 15.1 MeV location. This was a calibration point, though close investigation reveals the challenge of using this point for calibration: the photopeak is blurred beyond recognition. The shift in the unfolded location of the peak either resulted from improper selection of the peak location or inability of the algorithm to find it.

4.3.4 Propagation of Statistical Error

The method described in Section 3.3 is used to propagate the statistical error through the unfolding process. Both the source and background counts are Poisson distributed,

but to subtract the background, they are converted to count rates. Propagating the statistical error for each leads to Eq. 15 for the variance of the gross count rate

$$S_x^2 = \frac{n}{t_n^2} + \frac{b}{t_b^2} \tag{15}$$

where S_x is the standard deviation of the gross count rate in a bin, n is the number of source counts in a bin, n is the measurement time for the source, b is the number of background counts in a bin, and t_b is the measurement time for the background. These are then unfolded with a matrix B, such that each element is the square of each corresponding element in R.

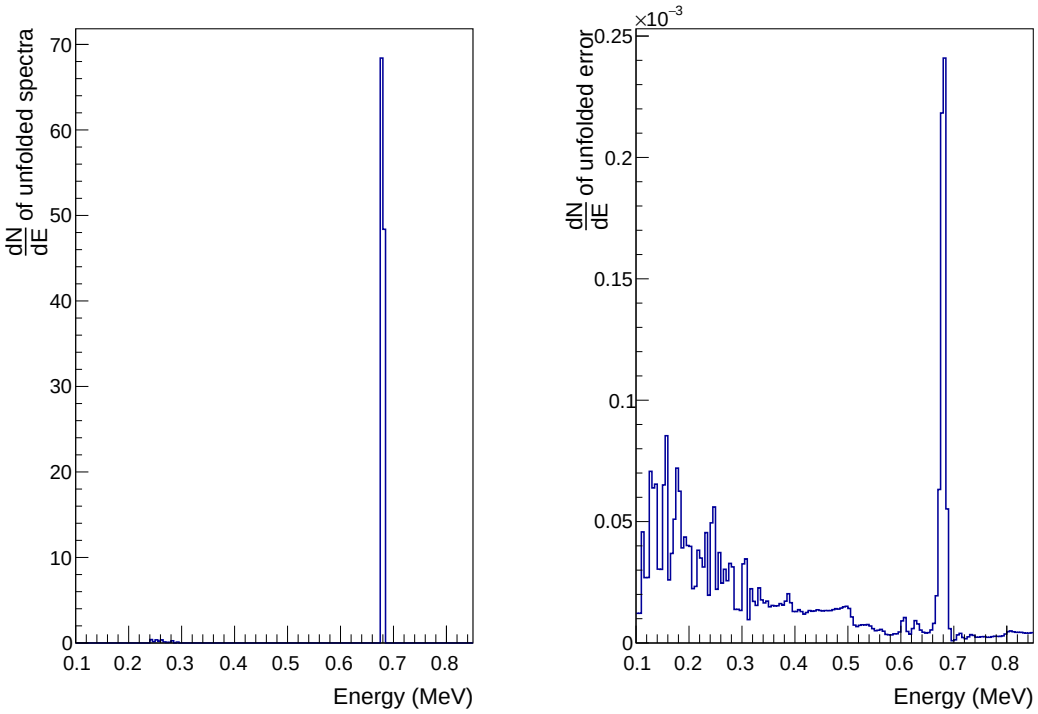

(a) Unfolded ^{137}Cs spectrum

(b) Error of unfolded ^{137}Cs spectrum

Figure 21: A comparison of the unfolded spectrum to its corresponding statistical error shows they are 5 orders of magnitude apart.

A sample of this propagation is shown in Figure 21 for ^{137}Cs. It is clear from these plots why the error bars are not visible: they are 5 orders of magnitude smaller than the unfolded spectra.

CHAPTER V

CONCLUSIONS AND FUTURE WORK

Due to the pervasive nature of gamma spectroscopy across so many fields of study, having adequate tools for analyzing the resulting spectra is essential. The original motivation of this work was to unfold and characterize the gamma measurement from a $^{11}B(d,n\gamma)^{12}C$ reaction. The resulting information is to be used in simulation of the source for nonproliferation research. Along the way, many interesting questioned seemingly raised themselves due to the nature of the problem and the methods selected.

5.1 The Response Function

Using Monte Carlo methods to create the response function for the unfolding presented both advantages and disadvantages. One benefit is that these simulations are not limited in energy-space. They can simulate any monoenergetic photon and its resulting energy deposition in a detection volume. This is helpful for both filling in the response function more finely and extending to energies beyond the capabilities of any of the sources available at Georgia Tech. The obvious limitation is the detail and complexity of the model and its implications on the results. It is not immediately evident to what degree the model should represent reality. This work revealed that something like adding a room around the experiment makes a slight change in the spectrum, but adding a gram of metal around the source drastically changes the response.

This leads to another important point raised by this research: the details of the unfolding are entirely dependent on the desired outcome of the code. For example, creating a response function that unfolds the energy distribution that is directly

incident upon the detector, a response function that unfolds the energy distribution leaving the source within some small time window, or a response function that unfolds the true nuclear transition probabilities are three very different problems. In the case of a high activity source, the response function used in this thesis cannot possibly represent such a situation given the structure of the simulation, begging the question: what does the unfolded result physically mean? In a response function where one gamma is simulated after another, no pile-up or background coincidence can occur.

Accounting for the temporal behavior of the source and the possible coincidence of background would make the response function a more accurate representation. For a given event, depending on the provided activity, the number of gammas produced are sampled from a PDF characteristic of its decay rate. Similarly, with a given probability, one or more background counts could be registered in the detector simultaneously with a source count. These types of counts are not linearly separable, an assumption these unfolding methods depend on. This, of course, raises another problem: this response function is only suitable for one activity level and one background spectrum (the price to pay for sophistication).

5.2 The Algorithm

Gold's iterative unfolding method was designed decades ago for this exact purpose: gamma spectrum deconvolution. It truly shines when unfolding a spectrum with distinct peaks. But given a bremsstrahlung spectrum, it quickly breaks down. This is fine for conventional gamma sources, but in more complex energy fields such as fission, bremsstrahlung, or nuclear-reaction-broadened peaks, the algorithm does not maintain the continuity. Although this work exclusively uses this algorithm for unfolding, this is not to say it is what is most appropriate. Some algorithms common to neutron spectral unfolding are build to deal with much more ill-conditioned problems and could likely be of use in unfolding continuous spectra.

The algorithm does have the benefit of guaranteeing convergence to some sharp spectrum given high enough parameters. This matter is discussed more in the next section.

Mentioned briefly in the introduction was some work on using machine learning for unfolding. The current literature is littered with attempts at gamma and neutron unfolding using neural networks and the like. I believe there is still work to be done in the field, and using combinations of the response function generation techniques discussed above paired with machine learning could prove fruitful. The response function approach becomes training set generation, and unfolding something nonlinear like the nuclear transition probabilities becomes more realistic. Such an approach requires a strict selection of the training data to be confident in the result.

5.3 Evaluating the Performance

One of the most challenging aspects of this work is in the selection of the unfolding parameters and evaluation of unfolded spectra. Even the measure of the quality of the unfolding is brought into question. As was mentioned, the 2-norm of the residual is used consistently, but this has the effect of choosing the spectrum that satisfies $y = Rx$ closely. The underlying problem is revealed during the model evaluation: there exist discrepancies between model and measurement. In future studies, this measure of performance needs to be examined and chosen with more regard to the physical implications of the selection. One solution is to simply take the 2-norm of the residual of only regions where the model is in good agreement.

The other difficulty in the evaluation is that the parameter space is large and required some heuristic truncating. The performance reported by each parameter set selection was inherently biased by the performance metric. What can be concluded from this study is that beyond a certain number of iterations, the algorithm essentially converges and does not perform any better (or worse). Having higher boosting and

repetition values sharpened the peaks in the unfolded spectrum. If the boosting value was too high for the number of repetitions, several lines around a peak would form (and not combine to form one line). A similar phenomenon occurs with the contrary. The relationship between repetitions and boosting is nonlinear and even with some parametric studies, it seems the best approach is as such: decide a performance metric, test the algorithm with a large subset of parameter combinations and choose the best one.

APPENDIX A

PEAK BROADENING CALCULATIONS

The energy resolution at the 4.438 MeV characteristic gamma peak from PuBe is higher than anticipated in the $LaBr_3$(Ce) measurements. The kinematic calculations of the nuclear reactions occurring in PuBe that produce the gammas show that this is not a characteristic of $LaBr_3$(Ce) but of PuBe. First considering the (α, n) reaction with ^{9}Be, shown in Figure 22, we perform an energy and momentum balance to determine the resulting kinetic energy of ^{12}C*. The constant values are listed in Eq.

$$\begin{aligned} m_n &= 939.565\frac{MeV}{c^2} \\ m_\alpha &= 3728.401\frac{MeV}{c^2} \\ m_C &= 11177.928\frac{MeV}{c^2} \\ E_\alpha &= 5.245MeV \\ Q_{^9Be(\alpha,n)^{12}C*} &= 1.264MeV \\ Q_{\gamma-decay} &= 4.438MeV \\ m_{C*} &= 11182.366\frac{MeV}{c^2} \end{aligned} \tag{16}$$

We only consider the case where the ^{12}C* is emitted forward because this is the maximum kinetic energy of ^{12}C*. In this case, the gamma emitted will be at a maximum when in the same direction as ^{12}C* and minimum when emitted opposite of ^{12}C*.

$$E_\alpha + E_{Be} + Q_{^9Be(\alpha,n)^{12}C*} = E_n + E_{C*} \tag{17a}$$

$$p_\alpha + p_{Be} = p_{C*} - p_n \tag{17b}$$

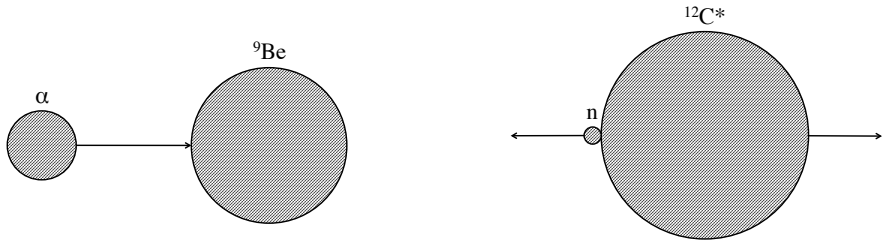

Figure 22: The (α, n) reaction in PuBe results in a neutron and a ^{12}C. The gamma will achieve maximum and minimum energies when the reaction occurs with the α at maximum energy.

$$E_\alpha + \cancelto{0}{E_{Be}} + Q_{^9Be(\alpha,n)^{12}C*} = \frac{p_n^2}{2m_n} + \frac{p_{C*}^2}{2m_{C*}} \tag{18a}$$

$$p_n = p_{C*} - \sqrt{2m_\alpha E_\alpha} + \cancelto{0}{p_{Be}} \tag{18b}$$

$$\frac{(p_{C*} - \sqrt{2m_\alpha E_\alpha})^2}{2m_n} + \frac{p_{C*}^2}{2m_{C*}} - E_\alpha - Q_{^9Be(\alpha,n)^{12}C*} = 0 \tag{19}$$

$$\left(\frac{1}{2m_n} + \frac{1}{2m_{C*}}\right) p_{C*}^2 - \frac{\sqrt{2m_\alpha E_\alpha}}{m_n} p_{C*} + \left(\frac{m_\alpha E_\alpha}{m_n} - E_\alpha - Q_{^9Be(\alpha,n)^{12}C*}\right) = 0 \tag{20}$$

$$\begin{aligned} p_{C*} &= 246.486 \frac{MeV}{c} \\ E_{C*} &= 2.717 MeV \end{aligned} \tag{21}$$

With the ^{12}C* nucleus traveling at 2.717 MeV, the maximum gamma energy will be when it is emitted in the opposite direction of the original momentum of ^{12}C*. Conversely, the minimum gamma energy will be when it is emitted in the same direction. We determine these gamma energy bounds by doing an energy and momentum balance for both cases.

For the maximum case:

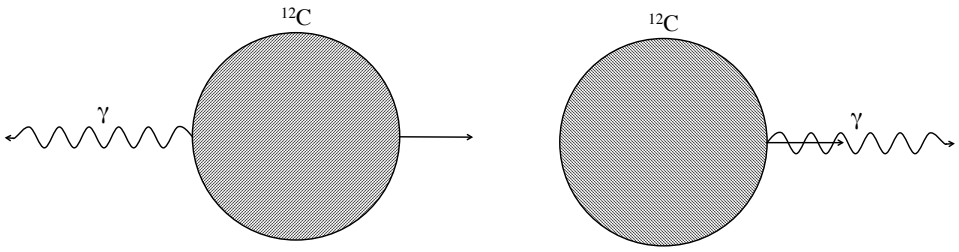

Figure 23: The gamma decay of the carbon yields the maximum and minimum gamma energies when it is emitted forward or backwards, respectively. The carbon should also be moving at its maximum energy.

$$Q_{\gamma-decay} + E_{C*} = E_C + E_\gamma \tag{22a}$$

$$p_{C*} = p_C - p_\gamma \tag{22b}$$

$$Q_{\gamma-decay} + E_{C*} = \frac{p_C^2}{2m_C} + p_\gamma c \tag{23a}$$

$$p_C = p_{C*} + p_\gamma \tag{23b}$$

$$Q_{\gamma-decay} + E_{C*} = \frac{(p_{C*} + p_\gamma)^2}{2m_C} + p_\gamma c \tag{24}$$

$$\left(\frac{1}{2m_C}\right) p_\gamma^2 + \left(\frac{p_{C*}}{m_C} + c\right) p_\gamma + \left(\frac{p_{C*}^2}{2m_C} - Q_{\gamma-decay} - E_{C*}\right) \tag{25}$$

$$\begin{aligned} p_\gamma &= 4.536 \frac{MeV}{c} \\ E_\gamma &= 4.536 MeV \end{aligned} \tag{26}$$

For the minimum case:

$$Q_{\gamma-decay} + E_{C*} = E_C + E_\gamma \tag{27a}$$

$$p_{C*} = p_C + p_\gamma \tag{27b}$$

$$Q_{\gamma-decay} + E_{C*} = \frac{p_C^2}{2m_C} + p_\gamma c \tag{28a}$$

$$p_C = p_{C*} - p_\gamma \tag{28b}$$

$$Q_{\gamma-decay} + E_{C*} = \frac{(p_{C*} - p_\gamma)^2}{2m_C} + p_\gamma c \tag{29}$$

$$\left(\frac{1}{2m_C}\right) p_\gamma^2 + \left(c - \frac{p_{C*}}{m_C}\right) p_\gamma + \left(\frac{p_{C*}^2}{2m_C} - Q_{\gamma-decay} - E_{C*}\right) \tag{30}$$

$$\begin{aligned} p_\gamma &= 4.340 \frac{MeV}{c} \\ E_\gamma &= 4.340 MeV \end{aligned} \tag{31}$$

REFERENCES

[1] *Proc. Nuclear Science Symposium Conference (Norfolk, Viginia, October 30 - November 5, 1994)*, vol. 1 of *Gamma Spectral Analysis via Neural Networks*, IEEE, 1994.

[2] *Nuclear-Reaction-Based Radiation Source for Explosives-And SNM-Detection in Massive Cargo*, vol. 1336 of *Application of accelerators in research and Industry: Twenty-First International Conference*, AIP Publishing, 2011.

[3] Ajzenberg-Selove, F., , and Kelley, J. H., "Nuclear data sheets," vol. NP A506, 1990. Data extracted from the ENSDF database, 2016.

[4] Brun, R. and Rademakers, F., "Root - an object oriented data analysis framework," *Proceedings AIHENP'96 Workshop, Lausanne, Sep. 1996, Nucl. Inst. and Meth. in Phys. Res. A*, vol. 389, pp. 81–86, 1997.

[5] Dorenbos, P., de Haas, J. T. M., and van Eijk, C. W. E., "Non-proportionality in the scintillation response and the energy resolution obtainable with scintillation crystals," *IEEE Transactions on Nuclear Science*, vol. 42, no. 6, 1995.

[6] Gold, R. and Bennett, E. F., "Error estimates for iterative unfolding," *Journal of Computational Physics 3*, vol. 3, pp. 167–175, 1968.

[7] Gold, R., "An iterative unfolding method for response matrices," technical report, Argonne National Lab., III, 1964.

[8] Guttormsen, M., Tveter, T., Bergholt, L., Ingebretsen, F., and Rekstad, J., "The unfolding of continuum y-ray spectra," *Nuclear Instruments and Methods in Physics Research*, vol. 374, pp. 371–376, 1996.

[9] Iltis, A., Mayhugh, M., Menge, P., Rozsa, C., Selles, O., and Solovyev, V., "Lanthanum halide scintillators: Properties and applications," *Nuclear Instruments and Methods in Physics Research A*, vol. 563, pp. 359–363, 2006.

[10] Jandel, M., Morhac, M., Kliman, J., Krupa, L., Matousek, V., Hamilton, J., and Ramayya, A., "Decomposition of continuum y-ray spectra using synthesized response matrix," *Nuclear Instruments and Methods in Physics Research*, vol. 516, pp. 172–183, 2004.

[11] Knoll, G. F., *Radiation Detection and Measurement*. John Wiley & Sons, Inc., 4 ed., 2010.

[12] Mitchell, T. M., *Machine Learning*. The McGraw-Hill Companies, Inc., 1997.

[13] Morhac, M., Kliman, J., Matousek, V., Veselky, M., and Turzo, I., "Efficient one- and two-dimensional gold deconvolution and its application to y-ray spectra decomposition," *Nuclear Instruments and Methods in Physics Research Section A*, vol. 401, pp. 385–408, 1997.

[14] Prussin, S. G., *Nuclear Physics for Applications: A Model Approach*. Wiley-VCH Verlag GmbH & Co. KGaA, Weinheim, 2007.

[15] Quarati, F., Owens, A., Dorenbos, P., de Haas, J., Benzoni, G., Blasi, N., Boiano, C., Brambilla, S., Camera, F., Alba, R., Belli, G., Maiolino, C., Santonocito, D., Ahmed, M., Brown, N., Stave, S., Weller, H., and Wu, Y., "High energy gamma-ray spectroscopy with $labr_3$ scintillation detectors," *Nuclear Instruments and Methods in Physics Research A*, vol. 629, pp. 157–169, 2011.

[16] Rahman, M. S. and Cho, G., "Unfolding low-energy gamma-ray spectrum obtained with nai(tl) in air using matrix inversion method," *Journal of Scientific Research*, vol. 2, pp. 221–226, 2010.

[17] Rose, P. B., Erickson, A. S., Mayer, M., Nattress, J., and Jovanovic, I., "Uncovering special nuclear materials by low-energy nuclear reaction imaging," *Scientific Reports*, vol. 6, 2016.

[18] Rose, P. B., "Cherenkov detectors for transmission studies of monoenergetic high-energy photons in active interrogation," Master's thesis, Georgia Institute of Technology, December 2015.

[19] Trautmann, W., Sharpey-Schafer, J., Andrews, H., Haas, B., Häusser, O., Taras, P., and Ward, D., "Measurement of the linear polarization of continuum gamma rays from (32s, xn) reactions to prolate and oblate rare-earth nuclei," *Nuclear Physics A*, vol. 378, p. 141–158, 1982.